EUROPEAN FUSION DEVELOPMENT AGREEMENT

EFDA–JET–PR(04)51

E. Surrey, C.D. Challis, D. Ciric, S.J Cox, B. Crowley, I. Jenkins, T.T.C. Jones
D. Keeling and JET EFDA Contributors

Measurement of the Depletion of Neutraliser Target due to Gas Heating in the JET Neutral Beam Injection System

Measurement of the Depletion of Neutraliser Target due to Gas Heating in the JET Neutral Beam Injection System

E. Surrey, C.D. Challis, D. Ciric, S.J Cox, B. Crowley, I. Jenkins, T.T.C. Jones
D. Keeling and JET EFDA Contributor*

EURATOM/UKAEA Fusion Association, Culham Science Centre, Abingdon, OX14 3DB, UK
** See annex of J. Pamela et al, "Overview of Recent JET Results and Future Perspectives", Fusion Energy 2002 (Proc.19 th IAEA Fusion Energy Conference, Lyon (2002)).*

Preprint of Paper to be submitted for publication in
Fusion Engineering and Design

ABSTRACT

The reduction in neutralisation efficiency of positive ion beams compared to theoretical calculations has been acknowledged for some time. The effect has been ascribed to a depletion of the gas target in the neutraliser, although the cause of this has been the subject of debate. Recent measurements in the neutraliser of the JET Neutral Beam Injection system showed a significant increase of the gas temperature, supporting the gas heating hypothesis. This work presents direct measurement, by two methods, of the power contained in the neutral component of the JET neutral beam injection system that confirms the neutralisation shortfall. A calorimetric technique is used to compare the power within the full (i.e. ions and neutrals) and neutral beam components for the high current JET triode injectors, from which the effective gas target can be derived. The results of these measurements are confirmed by considering the response to neutral beam injection of the energy stored in the tokamak plasma. Finally, the gas heating model, combined with earlier measurements of the gas temperature in the neutraliser, is used to support the hypothesis that the target depletion is due to indirect heating of the neutraliser gas by the beam.

1. INTRODUCTION

High power, Neutral Beam Injection (NBI) systems are commonly employed as additional plasma heating tools on magnetically confined fusion devices. The JET NBI system consists of two Neutral Injection Boxes (NIBs) each equipped with up to eight Positive Ion Neutral Injectors (PINIs) [1]. There are three types of PINI currently in use, designated by the maximum operating voltage and beam current in deuterium: the “tetrode” 80kV/56A, the “triode” 140kV/30A and the recently upgraded “HC triode” 130kV/60A [2,3]. The NIB located at machine octant 4 (NIB4) is supplied with seven tetrode PINIs and one triode PINI, whilst the NIB located on octant 8 (NIB 8) is supplied with eight HC triode PINIs. It has long been established that the neutral beam power achieved by the positive ion based systems at JET falls short of the predicted value determined from the expected neutraliser gas target and the well known reaction cross sections. This problem is more acute for the upgraded HC triode PINIs on NIB8.

Recent spectroscopic measurements of the neutral gas temperature in the neutraliser cell [4], [5] performed on the JET Neutral Beam Test Bed, showed that the probable cause of this deficit was depletion of the gas target due to indirect heating by the beam. The consequence of this observation for the JET neutral beam injectors is a reduction of neutral beam power delivered to the plasma. Accurate knowledge of this quantity is necessary for interpretation of measurements made on the tokamak plasma itself, hence the requirement to confirm, by measurement, the extent of this effect.

The power contained within the neutral component of the beam can be inferred from calorimetric measurements of the total extracted beam power (referred to as un-deflected beam) and the power observed when the residual ionic species have been removed by a transverse

magnetic field (referred to as deflected beam). A second measurement of the neutral beam power can be obtained by comparing the response of the tokamak plasma to neutral beam injection from the 130kV injectors to that of injection from the lower power 80kV injectors, for which the neutral power is well established. Finally, the gas heating model of PamÈla [6], together with the measured gas temperatures and neutraliser plasma parameters [5] can be used to predict, via a revised neutraliser gas target, the neutral beam power. These three methods are described and the results compared in the following sections.

2. CALORIMETRIC MEASUREMENT OF NEUTRAL BEAM POWER

A plan view of a JET NIB is shown in Fig.1; the eight PINIs are vertically mounted in two banks of four. The ion beam extracted from the source is passed through a gas neutraliser and the subsequent mixed beam of ions and neutral particles passes through a deflection magnet. For injection into the tokamak, the magnet is energised to remove the unwanted ionic beam component and the neutral beam passes into the torus via the duct, as shown by the lower beam in Fig.1. For beam diagnostic purposes, however, the beam can be stopped before reaching the duct on a calorimeter, as shown by the upper beam. Note that the situation represented by Fig.1 is for illustrative purposes only; in normal operation both beams would either pass into the tokamak or be intercepted on the calorimeter.

The calorimeter consists of two assemblies, each of eight 30mm thick copper plates, two metres high, hinged in the vertical mid-plane of the NIB. Each plate is precision machined into 7×59 16mm square castellations, some of which contain thermocouples positioned 10mm below the front face, to form four horizontal arrays and one central, vertical array in each assembly. Each assembly presents an angle to the beam varying from 32 degrees at the beam fringes to 14.2 degrees at the beam centre line. The thermocouple arrays are normally used to determine beam distributions in the vertical and horizontal directions. For the purposes of determining the efficiency of the gas neutralisers, the response of the thermocouple arrays was used to measure the energy deposited on the calorimeter by the beam. A typical response of the vertical thermocouple array is shown in Fig.2(a), whilst Fig.2(b) shows the horizontal array for which the rise in temperature of each thermocouple has been normalised to the angle of incidence of the beam.

The vertical thermocouple array is entirely contained within the central element of the assembly and a typical thermocouple response with time is shown in Fig.3. To determine the beam power the energy, E, deposited on the central array, which is proportional to the average temperature rise, $\overline{\Delta T}$, of the element, is computed. However, the thermal time constant of the calorimeter in the direction along the vertical beam axis is approximately an order of magnitude greater than that in the horizontal direction (due to the much larger temperature gradient in the latter and the effect of the castellations) so that the element will not reach a uniform temperature within a convenient time scale. The average temperature rise across the whole element was therefore obtained from the expression:

$$\overline{\Delta T} = \frac{\sum_{i=1}^{N-1} \frac{1}{2}(\Delta T_{i=1} + \Delta T_i)\Delta y}{y} \quad (1)$$

where

ΔT_i is the rise in temperature of the i^{th} thermocouple in the vertical array, measured approximately 10s after the initial thermocouple response when steady heat flow during the cooling phase has been achieved as shown in Fig.3.

Δy is the separation between thermocouples in the vertical array

y is the total length of the vertical thermocouple array

N is the number of thermocouples in the element

Equation (1) gives less weight to the two end thermocouples (i=1 and i=21), in addition these are positioned 22mm inboard of the ends of the element, so that equation (1) does not include the contribution from this fraction of the calorimeter. In practice these two errors are not significant, as there is effectively zero beam flux at these two points, as shown in Fig 2(a).

The method depends upon the relative response of the thermocouples to two different beams. The effect of different beam widths is included by calculating the fraction, f, contained between x=±s of a gaussian beam of rms radius s, centred at x_0:

$$f = \int_{-\infty}^{\sigma} \frac{1}{\sigma\sqrt{2\pi}} \exp\left\{-\frac{1}{2\sigma^2}(X-X_0)^2\right\} \Big/ \int_{-\infty}^{-\sigma} \frac{1}{\sigma\sqrt{2\pi}} \exp\left\{-\frac{1}{2\sigma^2}(X-X_0)^2\right\} \quad (2)$$

where s and x_0 are determined from a gaussian fit to the data from the horizontal thermocouple array.

For the un-deflected beam, i.e. containing both ion and neutral components, the total energy, E_d, deposited on the calorimeter is the product of the extracted beam current, voltage, transmission and pulse duration. For the deflected beam, i.e. the neutral component only, the total energy deposited on the calorimeter is some fraction, h, of this product, where h defines the neutralisation efficiency of the neutraliser. By comparing the average temperature rise of the central element for deflected and un-deflected pulses with similar extraction parameters, the neutralisation efficiency can be determined from:

$$\eta = \frac{\overline{\Delta T_D} E_U f_U}{\overline{\Delta T_U} E_D f_D} \quad (3)$$

where the subscripts D and U denote deflected beam and un-deflected beam respectively.

The measured values of neutralisation efficiency, h, are shown in Fig.4 as a function of extracted beam voltage. Measurements were made for beams from the 130kV/60A upgraded triode PINIs (referred to as “HC Triode”). In un-deflected mode, the beam voltage is limited to 90kV to avoid excessive thermal loading of the calorimeter elements. Thus the neutralisation efficiency for deflected beams of energy greater than 90keV must be determined by comparison with un-

deflected beams at this maximum energy. It is therefore important that the horizontal gaussian width of the beam, x_g, is determined as accurately as possible, so that the fraction, f, in equation (2) is also determined accurately. This is best achieved by ensuring that the deflected beam measurements are always taken for beams of optimum perveance at the given energy, as this maximises the response of the central thermocouples in the horizontal array. It is also assumed that transmission losses in the beamline are identical for deflected and un-deflected operation. Figure 4 also shows the results of computation of the neutralisation efficiency using a line integrated, cold (i.e. room temperature) target density, P_C. The cold target is obtained from empirically derived formulae for the neutraliser pressure in the absence of extracted beam, corrected for the loss in contribution from the source flow represented by the extracted beam current and varies from 1.6×10^{20} at low beam current to 1.3×10^{20} molecules/m^2 at high beam current. The reduction in neutralisation efficiency with increasing beam voltage is clearly evident, falling to approximately 60% of the expected value at maximum voltage.

2.1. CALCULATION OF NEUTRALISER TARGET

The beam initially extracted from the source consists of three ionic species: D^+, D_2^+ and D_3^+. As the beam traverses the neutraliser target these evolve into full and partial energy neutral and ionic species. Furthermore, the ratio of the initial species varies with the arc current in the ion source(and hence extracted beam current); thus the composition of the final beam is a complex function of beam current. The processes included in the calculation are given in Table 1. The fraction, F_0, of the total beam power in the neutral component of a given species is calculated from a series of equations of the form:

$$\frac{dF_0}{d\Pi} = \sum \sigma_{10} F_1 - \sum F_0 \sigma_{01} \qquad (4)$$

where F_1 is the fraction of the total beam power in the ionic beam component of a given species

σ_{10} represents cross section for a particular neutral producing process

σ_{01} represents the cross section for a particular ion producing process

The total power in the neutral component of the beam is given by the sum of the fractions obtained from the equations represented by equation (4) after integration from zero to a specified target density.

To obtain the effective target in the neutraliser, the neutralisation efficiency measured at the calorimeter must be corrected for re-ionisation losses in the additional path length of 1.25m represented by the deflection magnet. The pressure in the magnet has been measured to be a constant fraction of the pressure in the NIB (as obtained from the empirical formula) and the re-ionisation of the neutral beam caused by this target is estimated by assuming that full, half and third energy neutrals have the same flux ratios as their corresponding ionic species in the source.

The neutralisation efficiency at the neutraliser is then given by:

$$\eta_N = \frac{\eta}{1-f_R} \tag{5}$$

where

$f_R = f_0(E)\exp(-\Pi_M\sigma_{01}(E)) + f_0(E/2)\exp(-\Pi_M\sigma_{01}(E/2)) + f_0(E/3)\exp(-\Pi_M\sigma_{01}(E/3))$

$f_0(E), f_0(E/2), f_0(E/3)$ are the estimated full, half and third energy neutral fractions

σ_{10} is the re-ionisation cross section at the respective energy

Π_M is the integrated gas target along the magnet path

Strictly, the absolute neutral fractions calculated at the end of the neutraliser, for an assumed neutraliser target should be used to calculate the re-ionisation fraction and hence an adjusted efficiency. The new efficiency should then be used to re-calculate the neutraliser target and the process repeated iteratively until convergence is obtained. However, it can be shown that the error introduced by adopting the non-iterative technique is negligible; the correction to the neutralisation efficiency due to re-ionisation is approximately 3%.

The initial ratios of the species concentrations were measured by Doppler shift spectroscopy [7, 8, 9] as a function of beam current and are shown in Figure 5. These, together with the system of equations (4) can be used to determine the target density required to fulfil the measured neutralisation efficiency. The calculated neutralisation efficiency is shown as a function of target density in Figure 6 for extracted deuterium beams of energies 40keV and 125keV. It is particularly important that the fractional energy components are included in the calculation at low beam currents, where the D_3^+ species is significant. Figure 7 shows the reduced target, as a fraction of cold target, obtained for the data of Fig 4, together with historical data from the former NIB 8 PINI type, designated “Triode”. The Triode PINI operated at 140kV/30A with similar cold target densities to the HC Triode PINI.

Whilst the upgraded NIB 8 PINIs show percentages of cold target of the order 35%, the previous NIB 8 Triode PINIs yield much larger percentages of the order 60%. It should be noted that, at low beam energy (below 70keV) the target is effectively infinite and the neutralisation efficiency is insensitive to relatively large changes in target as shown in Fig.6. At higher energies, the neutralisation efficiency does not become asymptotic until much higher target densities are attained. Therefore, it is impossible to define a target at low beam energies from the measured efficiency, merely a lower limit, as indicated by the bars in Fig.7. The absolute magnitude of the error for higher energy data depends upon the locus on the neutralisation efficiency vs. target density curve. In most cases, however, the large error is in the direction of increasing target density, with the error in the opposite direction being of the order 30%. At highest energies the gas target error is typically ±10%; some indicative error bars have been shown for the HC Triode.

The apparent reduction in neutralisation target has been acknowledged for some time and recent measurements [4, 5] have implied that it is due to the indirect heating of the gas by the beam. The results of reference [4] show that the neutral gas temperature in the neutraliser is most strongly a function of beam current, with only a weak dependency on beam energy. The reduction in gas target apparent in Fig 7 also demonstrates this behaviour as can be seen from Fig 8 which shows the data of Fig 7 now plotted as a function of the extracted beam current. The historical Triode data now almost lie on a single curve with the low energy (low current) HC Triode data. Although there is some degree of scatter in the data (due to the sensitivity of the neutralisation efficiency to target density), it is clear that the reduction in neutraliser target follows the same scaling as the gas temperature measured in [4].

3. MEASUREMENT OF NEUTRAL BEAM POWER FROM TOKAMAK PLASMA RESPONSE

The ability to measure the neutral beam power independently of the neutral beam diagnostics is particularly useful in confirming the neutralisation measurements described in Section 2. This can be realised by measurement of the stored plasma energy for beams of known injection power and those from the HC Triode PINIs. The reference beam was taken from the 80kV/56A (HC Tetrode) PINIs, since the neutralisation deficit in these injectors has been documented extensively and the neutral beam power known with reasonable accuracy [10].

A plasma that is heated both ohmically and by neutral beam injection at constant power will reach a steady state with a constant plasma energy and assuming that the heat flow is zero-dimensional (i.e. in considering power entering and leaving the plasma the heat flow paths are not modelled explicitly but are represented by global heating and energy confinement times), the balance equation is:

$$(P_{NB} - P_{SH}) + P_{\Omega} = P_{TL} \qquad (6)$$

where

P_{NB} is the power injected by neutral beam

P_{SH} is the shine through power of the neutral beam (i.e. power not deposited in the plasma)

P_W is the ohmic heating power

P_{TL} is the total power lost from the plasma

The total power lost by the plasma is related to the global energy confinement time by empirical scaling expressions. As part of the physics studies in support of ITER, several such scaling expressions have been generated based on databases for specific operating regimes such as L-mode and H-mode [11]. These expressions all take a similar form in which the confinement time, t, of the thermal plasma energy is expressed as a function of several plasma and tokamak parameters in the form:

$$\tau = C I^{\sigma_I} B^{\sigma_B} P_{TL}^{\sigma_p} n^{\sigma_n} M^{\sigma_M} R^{\sigma_R} \varepsilon^{\sigma_\varepsilon} \kappa^{\sigma_\kappa} = \frac{W_{th}}{P_{TL}} \quad (7)$$

where I is the plasma current, B is the toroidal magnetic field strength, n is the line averaged density, M is the average ion mass, R is the major radius, e is the inverse aspect ratio and k is the elongation. For a steady state, L-mode plasma heated only by neutral beam injection all the terms in the middle of equation (7) can be considered constant with the exception of the total power loss. Thus equation (7) reduces to:

$$\tau = K P_{TL}^{\sigma_p} \quad (8)$$

The thermal confinement time, in a steady state plasma, is also given by:

$$\tau = \frac{W_{th}}{P_{TL}} \quad (9)$$

where W_{th} is the thermal component of the plasma energy. Thus combining equation (8) and (9), the thermal plasma energy can be directly related to the power loss by:

$$W_{th} = K P_{TL}^{\sigma_p + 1} \quad (10)$$

The thermal energy, W_{th}, is obtained from the diamagnetic energy, W_{dia}, which is a combination of thermal and fast ion energies and is measured by the diamagnetic loop diagnostic [12]:

$$W_{dia} = W_{th} + \frac{3}{2} W_{perp} \quad (11)$$

W_{perp}, the component due to the motion of fast ions perpendicular to the magnetic field lines, is calculated from the code PENCIL [13] and the factor 3/2 is included to account for the parallel degree of freedom that is not included in the measurement. Thus, combining equations (6) and (10), the injected neutral beam power can be expressed in terms of the thermal energy:

$$[(P_{NB} - P_{SH}) + P_\Omega] = \left(\frac{W_{th}}{K}\right)^{\beta} \quad (12)$$

where

The shine-through power is obtained from the PENCIL code [12] and the ohmic power from standard tokamak diagnostics. Additional losses such as neutral beam fast-ion orbit losses, investigated using the TRANSP [14] tokamak analysis code, were shown to be negligible. Calculation of charge exchange losses using cross sections for hydrogen and the Stix model for

fast ion slowing down time [15] showed that total charge–exchange losses scale mainly with total beam power, compared to shine-through losses, which are sensitive to the beam energy. As the method compares reference and test beams of different energies, beam energy dependent mechanisms will influence the final results to a greater extent than power dependent terms. Test calculations showed that neglecting shine-through losses introduced an error of approximately 5% in the final result, whereas the effect of charge-exchange was negligible. The work presented here therefore includes the shine-through loss but omits the charge-exchange loss in the calculation.

3.1 EXPERIMENTAL METHOD

The basic technique is to compare the thermal stored energy component, W_{th}, measured for the test beam, extracted from the 130kV/60A HC Triode PINI, with that of the reference beam extracted from the 80kV/56A HC Tetrode PINI. To achieve this, beams of 2 seconds duration from each PINI type were consecutively injected into suitable JET plasmas. The beam pulse duration ensured that a steady state would be obtained in each of the injection phases.

The technique required specific properties of the JET plasma, viz:-

(i) a minimum plasma density of $2\times10^{19}m^{-3}$

(ii) L-mode plasma throughout the heating phase

(iii) no other additional heating or fuelling technique, such as Ion Cyclotron Resonance Heating (ICRH), Lower Hybrid Current Drive (LHCD) or pellet refuelling

(iv) the tokamak plasma to be in steady state (steady plasma shape,

$dn_e/dt \sim 0$, $dW/dt \sim 0$, $dI/dt \sim 0$, $dB/dt \sim 0$, $d\,\overline{\ }_i/dt \sim 0$, $\overline{\ }_i$ is the plasma internal inductance) for at least 1 second before neutral beam injection.

The condition for the application of equation (8) has already been discussed (that all the quantities on the right hand side of equation (7) with the exception of the total power loss be constant) and the validity of this was checked for each neutral beam injection phase of the pulse. The ITER-96P L-mode scaling [10] allows the constant terms in middle of equation (7) to be displayed as a single quantity and gives $\alpha_P = -0.73$. Thus a confinement time, $\tau_{ITER96PL}$, normalised to $P^{-0.73}$ can be calculated, which should be constant throughout the beam injection phase of the plasma. Figure 9 shows a plot of this quantity, for a typical pulse, together with the diamagnetic loop measurement of W_{dia} and the injected neutral beam power, demonstrating that the conditions are satisfied. The time axis in Figures 9 to 11 refers to the time elapsed from the initiation of the JET plasma, which is taken as time zero. (It should be noted that the neutral beam power, P_{NB}, in Fig.9 has been obtained by using the average cold target described in Section 5 to calculate P_{NB}).

A series of twelve measurements were made with the reference PINIs operating at nominally 80kV and the extraction voltage of the test PINIs varied from 100kV to 115kV. Figure 10 shows

all the relevant quantities measured during a typical pulse. The reference PINIs inject first between 15 and 17 seconds after initiation, followed by the test PINIs between 17 and 19 seconds. The neutral beam power in Fig 10 is calculated from the known target in the reference PINI, P_{ref}, and from the average cold target described in Section 5 for the test PINIs, P_{test}.

The effect of high voltage breakdowns can be seen in the neutral beam power and for this reason the average power, $<P_{ref}>$, $<P_{test}>$ has been calculated during the time that the plasma is in steady state. Similarly the value of W_{dia} is only taken between 15.7s and 16.9s in the reference PINI pulse and between 17.5s and 18.8s in the test PINI pulse. Figure 10 also shows the shine-through power, P_{SH}, the ohmic heating power, P_W and the fast ion energy, $3W_{perp}/2$.

The quantities in equation (12) can now be calculated from the averaged values of Fig 10 and these are shown in Fig.11 for two different neutral beam pulses. In Fig.11(a) the value of the averaged steady state thermal energy, W_{th}, is almost constant in the reference and test pulse phases, despite a difference in the calculated absorbed neutral beam power of approximately 1MW. In Fig 11(b), a slight reduction in the calculated absorbed neutral beam power between the test and reference pulse phases is accompanied by a slight *increase* in the plasma thermal energy. These plots serve to illustrate that the cold target calculation overestimates the transmitted neutral beam power for the test PINIs.

3.2 DETERMINATION OF CORRECTION FACTOR

The results of the plasma response experiment were analysed to obtain a neutral beam power delivered by the HC Triode PINIs that is consistent with that from the HC tetrode PINIs. Introducing a correction factor, A, for the neutral beam power delivered by the HC Triode PINIs, equation (12) can be used to equate the plasma response of the test and reference phases:

$$\frac{W_{th,ref}^{\beta}}{P_{NB,ref} - P_{SH,ref} + P_{\Omega,ref}} = \frac{W_{th,test}^{\beta}}{A(P_{NB,test} - P_{SH,test}) + P_{\Omega,test}} \qquad (13)$$

Where the subscript “ref” refers to the reference (HC Tetrode) data and the subscript “test” refers to the test (HC Triode) data. Thus the correction factor can be expressed in terms of the measured quantities and the parameter β. Over the small range in voltage, the variation A is expected to be small and β can be taken as constant. Thus A and b may be determined by varying the latter and requiring a minimum standard deviation from the mean in the resultant values of A. This method gave values of $A = 0.81$ and $\beta = 0.66$ or $\alpha_p = 0.51$, which is close to early L-mode scalings such as Goldston [16] and ITER89L-P [17]. The parameter b could have been obtained from one of the scaling expressions relevant to the plasma regime in which the experiments were performed. However, these empirical scaling expressions are derived from a wide range of plasma conditions, thus there is considerable risk of introducing error into results derived from an experiment necessarily performed over a limited range of conditions. Secondly, uncertainties in the absolute magnitude of W_{dia}, including offsets, can appear as an error in the determination

of a_P. However the effect of such measurement uncertainties on the derived value of A is minimised in the region •••• of the data set.
Having determined A and b it is possible to display the results graphically by plotting ΔW_{th} against •••• where:

$$\Delta W_{th} = W_{th,test} - W_{th,ref} \tag{14a}$$

and

$$P_{netX} = P_{PBX} - P_{SHX} + P_{\Omega X} \qquad X = ref, test \tag{14b}$$

This is shown in Fig.12 for the corrected and uncorrected HC Triode neutral beam power. As can be seen the linear fit calculated from the uncorrected HC Triode neutral beam power does not pass through the origin, unlike that calculated from the corrected powers. This lends confidence in the analysis method, since this expected result is not automatically enforced by the algorithm.

4. RESULTS OF NEUTRALISER GAS HEATING MODEL

The gas heating model of PamÈla [6] has been applied to the neutraliser measurements of [4] and [5] and is described in detail in [5]; it can be used to predict the thermal gas temperature for a known neutraliser gas pressure, beam energy and current. For convenience of mounting on the NIB, the neutraliser cell is divided into two parts of 0.86m and 1m lengths respectively, the neutraliser gas being introduced at their junction. The pressure distribution through the neutraliser, in the absence of beam, has been measured by a moving ion gauge and takes the form shown in Fig.13. Using this distribution and the calculated line integrated cold target an effective pressure for the neutraliser can be obtained as input to the model. For a given beam energy and current, the thermal gas temperature, T_H, can be calculated and a value for the hot target, P_H, derived from a suitable scaling law.

It is known that the gas flow in the neutraliser is in the transition flow regime, for which the conductance effectively scales with the square root of the gas temperature (this scaling would also apply to the molecular flow regime) and on this basis it might be expected that the target density, which is proportional the gas number density would scale as $T^{-1/2}$, assuming that the *mass* flow is conserved. A series of measurements made on the neutraliser of a PINI in the Neutral Beam Test Bed, however, revealed that the neutraliser pressure, p_N, is constant over a wide range of beam powers as shown in Fig.14. This data was obtained by measuring the pressure, p_B, in a baratron situated at the end of a long, narrow bore connection such that the conditions for thermal transpiration were satisfied. Using the gas temperature, also shown in Fig.14, obtained by a fit to data obtained from spectroscopic measurement, the pressure in the neutraliser was calculated by the scaling law:

$$\frac{P_N}{P_B} = \sqrt{\frac{T_N}{T_B}} \qquad (15)$$

where

T_B=293K is the gas temperature in the baratron

T_N is the gas temperature in the neutraliser measured spectroscopically [4]

This behaviour indicates that the correct scaling for the hot target is in fact linear, i.e.:

$$\frac{\Pi_H}{\Pi_C} = \frac{T_C}{T_H} \qquad (16)$$

where T_C is the thermal temperature of the gas in the absence of beam i.e. ambient. The results are shown in Fig 8 expressed as a fraction of the cold target; comparison with the values derived from the neutralisation measurements shows reasonably good agreement, supporting the theory that target depletion is indeed due to gas heating. The reason for the apparent conservation of pressure is not obvious but is indicative of either an additional net sink term for the gas (presumably due to the implantation into the neutraliser walls of the neutraliser plasma ions, known as "ion pump-out") or subtle changes to the gas flow. Indeed a more thorough investigation of the data implies that, for beam power between 3MW and 6MW, the measured target is best fitted by assuming a scaling of $T^{-3/2}$, implying an even stronger sink term relative to the higher power beam. (It is most probable that the high power scaling represents a combination of ion pump-out and a source term due to gas evolution from the walls). However, as the higher current results are primarily of relevance to neutral beam injection at JET the linear scaling will be used for calculating the power transmitted to the plasma in Section 5.

5. CALCULATION OF POWER TRANSMITTED TO JET PLASMA

Calculation of the neutral beam power transmitted to JET requires accurate knowledge of the neutraliser gas target and the total beam losses along the beam path length. The latter have been estimated from calorimetric measurements to be 30% and historically, the former was taken to be a constant value of $6\times10^{19}m^{-2}$. This value was an attempt to adjust the design value of cold target ($1\times10^{20}m^{-2}$) for the observed, but un-quantified, target depletion, based upon the measured pressure distribution in the neutraliser shown in Fig.13 and indeed provided an adequate description of the HC Tetrode, Tetrode and Triode PINI performance. The predicted power transmitted to the JET plasma from a single HC Triode PINI under these conditions is shown as the dotted line in Figure 15.

Using the target densities obtained in Section 2, the revised transmitted neutral power can be calculated and these are shown as points on Fig.15 as a function of the total beam power extracted from single HC Triode PINI. The increasing shortfall with extracted power due to the depletion of the neutraliser target is obvious. Figure 15 also shows data from the plasma response experiment corresponding to extraction voltages of 100kV and 115kV. Finally, the solid curve shows the

predicted power based on the hot target derived from the gas heating model.

The gas heating model and the neutralisation measurements show reasonable agreement, as might be expected from the similarity of the gas depletion calculations, confirming the cause of target depletion. That the value of the transmitted neutral beam power taken from the plasma response measurements is also in agreement confirms that the neutralisation measurement technique is valid.

CONCLUSION

Two independent experimental techniques have shown that the neutral beam power transmitted to the JET plasma by the upgraded HC Triode (130kV/60A) PINI is below the value expected based on historical computation. Direct measurement of the neutralisation efficiency of the JET beams has enabled calculation of the effective target in the neutraliser as a function of beam parameters. It has been shown that the gas target can be depleted by up to 70% of the expected value and that the depletion is a strong function of beam current. Comparison with the gas heating model indicates that the depletion is indeed due to the indirect heating by the beam of the neutraliser gas. A revised computation of the neutral beam power transmitted to the JET plasma by the HC Triode PINI, based upon the measured, depleted target shows good agreement with measurement of neutral beam power based upon the plasma response. This has increased confidence in the gas heating model, which has been used to identify a method by which the target depletion can be reduced and this will be the subject of a subsequent publication.

ACKNOWLEDGEMENT

This work has been conducted under the European Fusion Development Agreement and funded by EURATOM.

REFERENCES

[1]. Duesing G. *et al.,* Fusion Technology **11** (1987) 163

[2]. D. Ciric, *et al* Proc. 19th Symp. On Fusion Engineering (2002) p140

[3]. Surrey E., Ciric D., Godden D. J. and Crowley B. Proc. 19th Symp. On Fusion Engineering (2002) p64

[4]. Surrey E. and Crowley B .2003 Plasma Phys Control Fusion **45** (2003), 1209

[5]. Crowley B., Surrey E., Cox S. J., Ciric D. and Ellingboe A R, Fus Eng and Design, **66-68**, Part A (2003) 591

[6]. Paméla J., Rev. Sci. Instrum. **57** (1986) 1066

[7]. Stork D and Hemsworth R S, Proc 8th Symp. on Eng. Problems of Fus. Res., San Francisco, (1979), 1024

[8]. Bonnal J.F., Bracco G., De Michelis C., Druaux J., Mattioli M., Oberson R. and Ramette J., Phys Lett, (1979) p65

[9]. Burrell C., Cooper W.S., Smith R R and Steele W.F., Rev. Sci. Instrum., 1980, 1451
[10]. Falter H.D., Ciric D., Cox S.J. and Godden D., “60kV Hydrogen Neutralisation Scan”, JET-R(98)10, JET Joint Undertaking, Culham Science Centre (1998)
[11]. ITER Physics Basis, Ch. 6, Nuclear Fusion **39** (1999)
[12]. Tonetti G., Christiansen J.P. and De Kock L., Rev. Sci. Instrum. **57** (1986) 2087
[13]. Challis C.D., *et al.,* Nuclear Fusion, **29**, (1989), 563
[14]. Budny R.V., *et al.*, Nuclear Fusion, **32**, (1992) 429
[15]. Stix T.H., Plasma Physics, **14** (1972) 367
[16]. Goldston R.J., Plasma Phys. Control. Fusion, **26**, (1984)87
[17]. Yushmanov P.N. et al, Nucl. Fusion, **30** (1990) 1999

Table 1 Collision Processes Included in the Calculation of Neutralisation Efficiency

Double (dissociative) ionisation	H	$+ H_2$	$\rightarrow$	$H + (H^+ + H^+) + 2e$
Double ionsiation with stripping	H	$+ H_2$	$\rightarrow$	$H^+ + (H^+ + H^+) + 3e$
Projectile electron loss	H	$+ H_2$	$\rightarrow$	$H^+ + H_2 + e$
Electron capture with ionisation	H	$+ H_2$	$\rightarrow$	$H^- + (H^+ + H^+) + e$
Electron capture by H	H	$+ H_2$	$\rightarrow$	$H^- + H_2^+$
Electron capture byH^+	H^+	$+ H$	$\rightarrow$	$H + H^+$
Electron capture by H^+	H^+	$+ H_2$	$\rightarrow$	$H + H_2^+$
Double electron capture by H^+	H^+	$+ H_2$	$\rightarrow$	$H^- + 2H^+$
Electron detachment	H^-	$+ H_2$	$\rightarrow$	$H + H_2 + e$
Double electron detachment	H^-	$+ H_2$	$\rightarrow$	$H^+ + H_2 + 2e$
Production of fast H from fast H_2	H_2	$+ H_2$	$\rightarrow$	H (fast, total)[a]
Production of fast H^+ from fast H_2	H_2	$+ H_2$	$\rightarrow$	H^+ (fast, total)[a]
Production of fast H_2^+ from fast H_2	H_2	$+ H_2$	$\rightarrow$	H_2^+
Total destruction of fast H_2	H_2	$+ H_2$	$\rightarrow$	(Destruction of H_2)[b]
Dissociation of fast H_2^+	H_2^+	$+ H_2$	$\rightarrow$	$(H^+ + H) + H_2$
Production of fast H from fast H_2^+	H_2+	$+ H_2$	$\rightarrow$	H (fast, total)[a]
Production of fast H^+ from fast H_2^+	H_2^+	$+ H_2$	$\rightarrow$	H^+ (fast, total)[a]
Electron capture by H_2^+	H_2^+	$+ H_2$	$\rightarrow$	$H_2 + H_2^+$
Total destruction of fast H_3^+	H_3^+	$+ H_2$	$\rightarrow$	(Destruction of H_3^+)[b]
Production of fast H from fast H_3^+	H_3^+	$+ H_2$	$\rightarrow$	H (fast, total)[a]
Production of fast H^+ from fast H_3^+	H_3^+	$+ H_2$	$\rightarrow$	H^+ (fast, total)[a]
Production of fast H_2 from fast H_3^+	H_3^+	$+ H_2$	$\rightarrow$	H_2 (fast, total)[a]
Production of fast H_2^+ from fast H_3^+	H_3^+	$+ H_2$	$\rightarrow$	H_2^+ (fast, total)[a]

[a] X (fast, total) indicates the sum of all processes leading to the creation of a fast species X

[b] (Destruction of X) indicates the sum of all processes leading to the destruction of species X

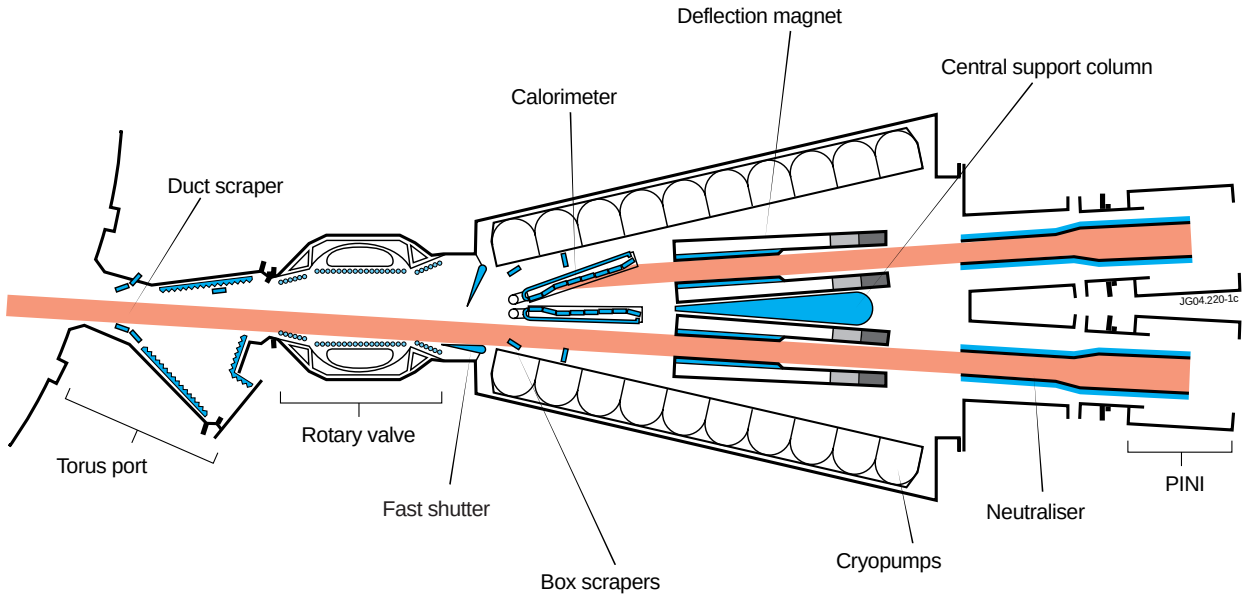

Figure 1: Plan view of the JET Neutral Injection Box.

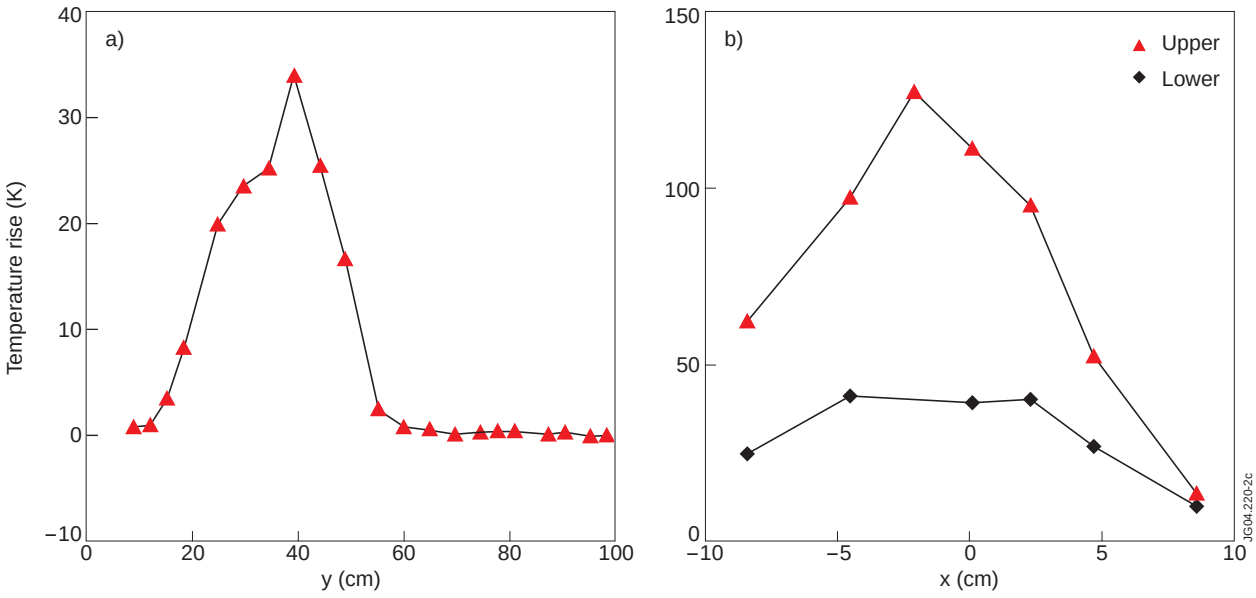

Figure 2: Beam profile measured by (a) the vertical thermocouple array in the calorimeter and (b) the horizontal thermocouple array. Temperatures in (b) are normalised to the angle of incidence of the beam.

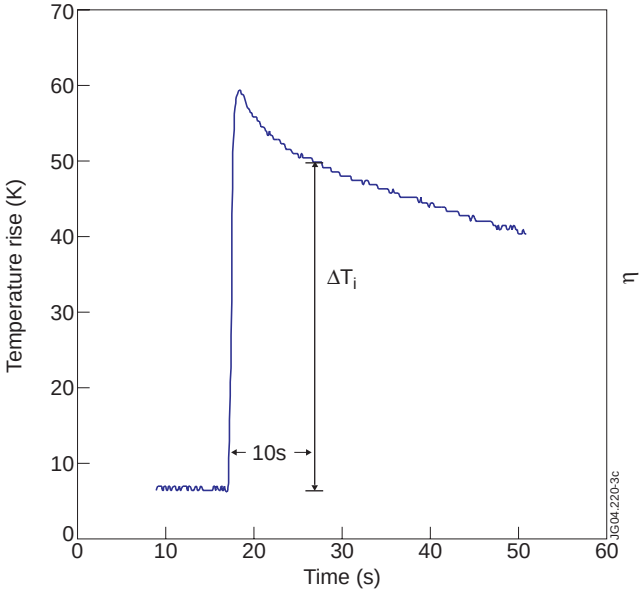

Figure 3: Time response of calorimeter thermocouple and definition of DT_i.

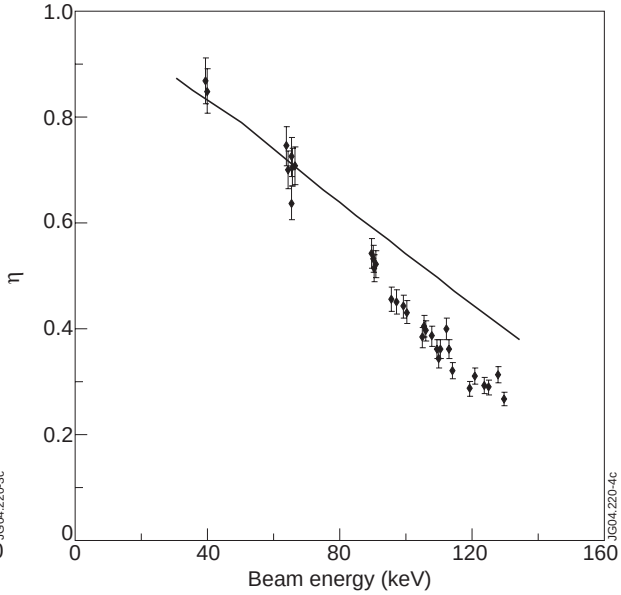

Figure 4: Neutralisation efficiency as a function of beam energy for the 130kV/60A triode PINI.: —— measured data; —◆— calculation from cold neutraliser target.

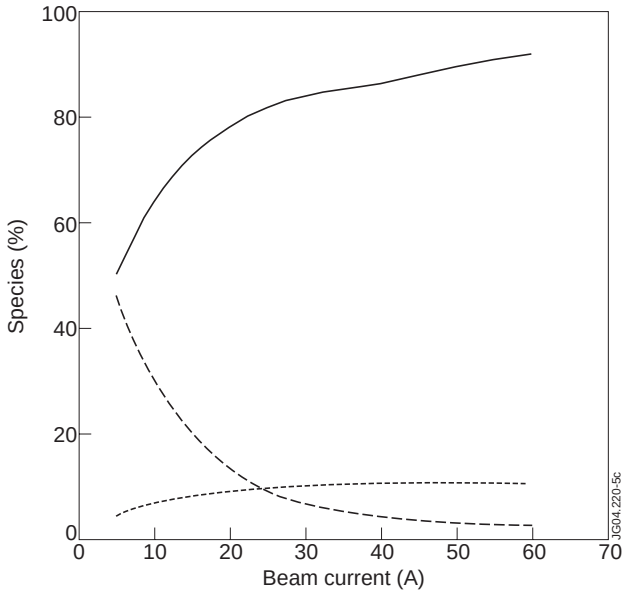

Figure 5: Ion species ratios in the PINI source as a function of beam current. —— D^+; ------- D_2^+; – – – – D_3^+

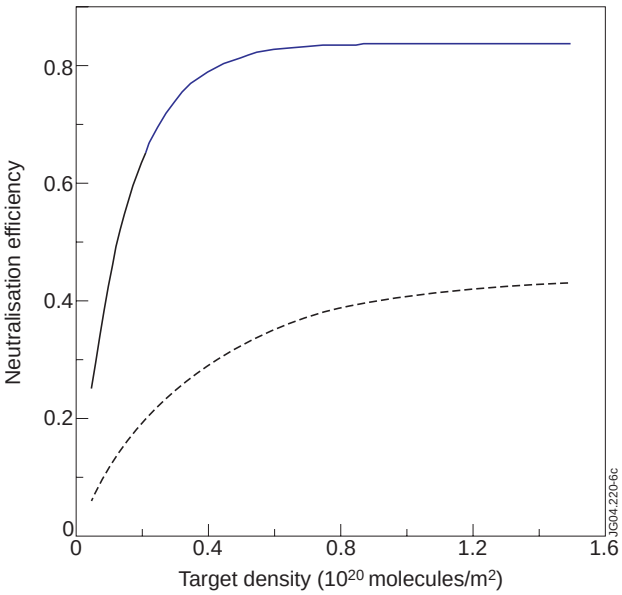

Figure 6: Theoretical neutralisation efficiency as a function of neutraliser gas target
—— *40keV/15A;* – – – – *125keV/53A*

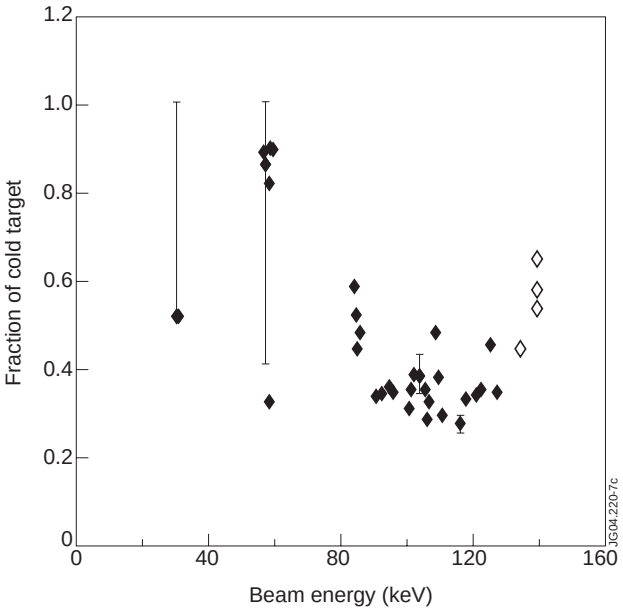

Figure 7: Measured neutraliser target expressed as a fraction of the calculated cold gas target for two types of PINI:. ◆ HC Triode; ◇ Triode

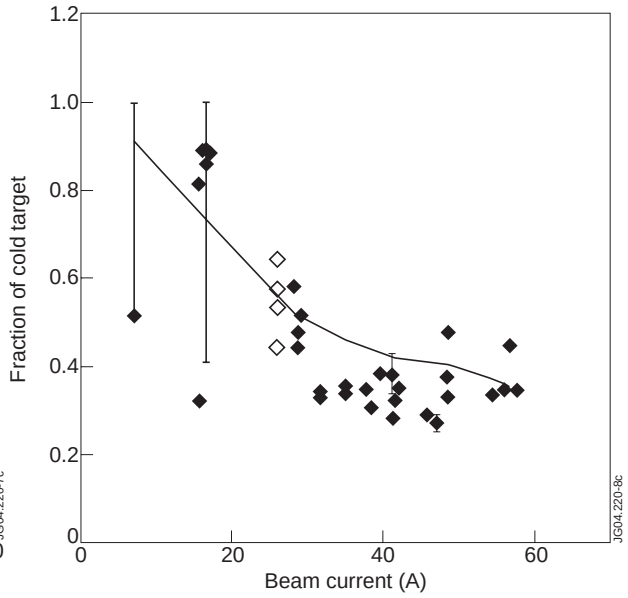

Figure 8: Measured neutraliser target expressed as a fraction of the calculated cold gas target as a function of beam current for two types of PINI: ◆ ◇ HC Triode;

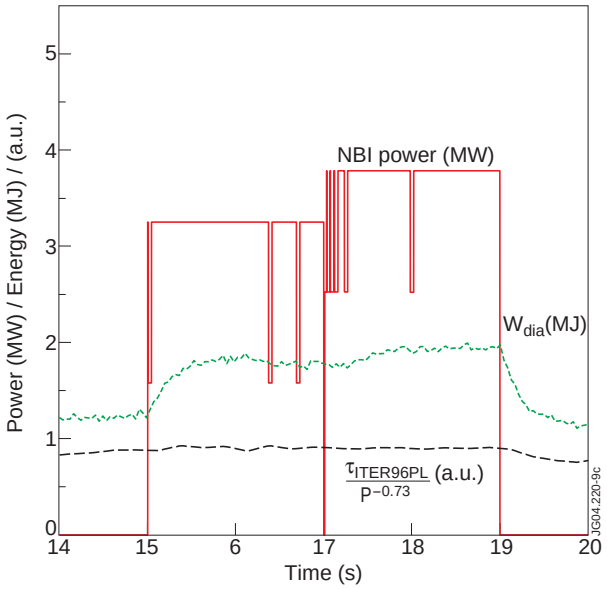

Figure 9: Demonstrating that the quantity $\tau_{ITER96PL} / P^{\alpha_P}$ *is constant during the steady state part of the beam injection phases. The time axis is time elapsed since initiation of the JET pulse at t=40s.*

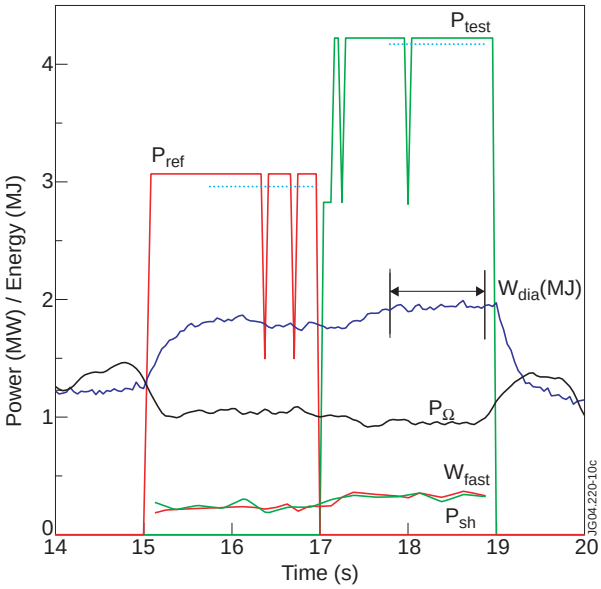

Figure 10: Data from typical plasma energy experiment pulse. Quantities are marked on figure except for . . . average NBI power from HC Triode (test) PINI and ------- average NBI power from HC Tetrode (ref) PINI.

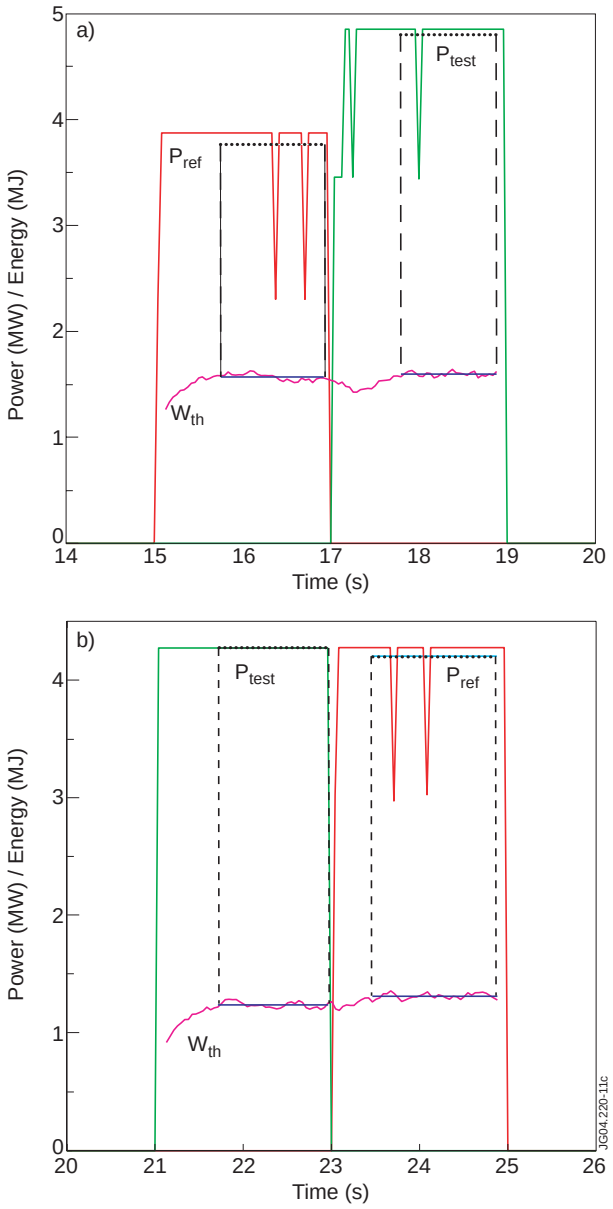

Figure 11: Two typical plasma energy pulses demonstrating the obvious over estimation of the neutral beam power calculation: (a) shows no significant change in W_{th}, despite an apparent increase in beam power in the second injection phase; (b) shows a slight increase in W_{th} in the second injection phase despite no significant change in beam power. The dashed lines indicate the limits of the steady state phase during which the method is valid. Quantities are marked on figure except for · · · average NBI power from HC Triode (test) PINI and ------- average NBI power from HC Tetrode (ref) PINI.

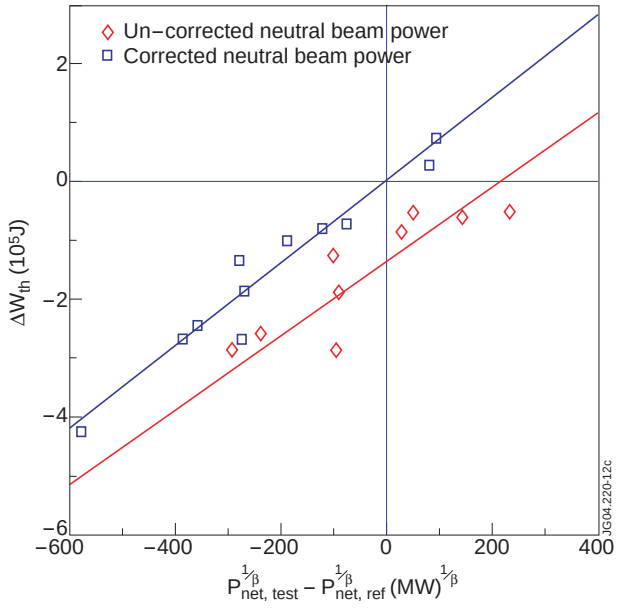

Figure 12: the change in W_{th} as a function of the change in absorbed power as calculated from the assumed gas target ◆ neutral beam power un-corrected; □ after correction factor, A, is applied to neutral beam power calculation.

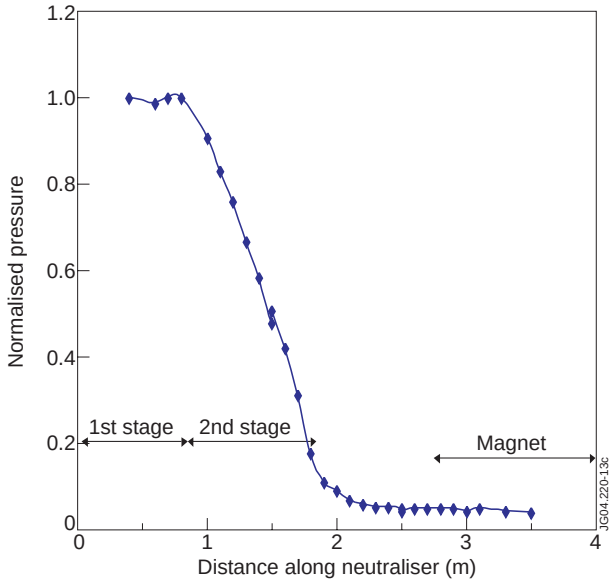

Figure 13: The measured, normalised pressure distribution along the neutraliser.

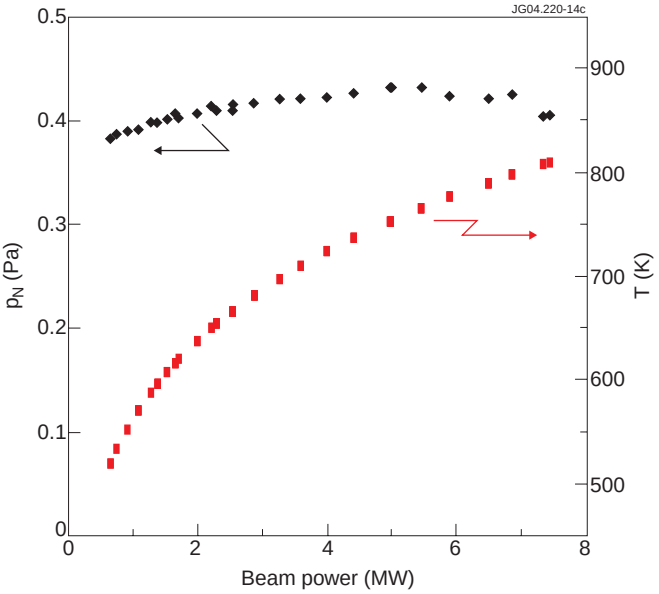

Figure 14: Results of the thermal transpiration experiment: ◆ neutraliser pressure measured by transpiration technique and □ neutral gas temperature in the neutraliser derived from a fit to data measured spectroscopically.

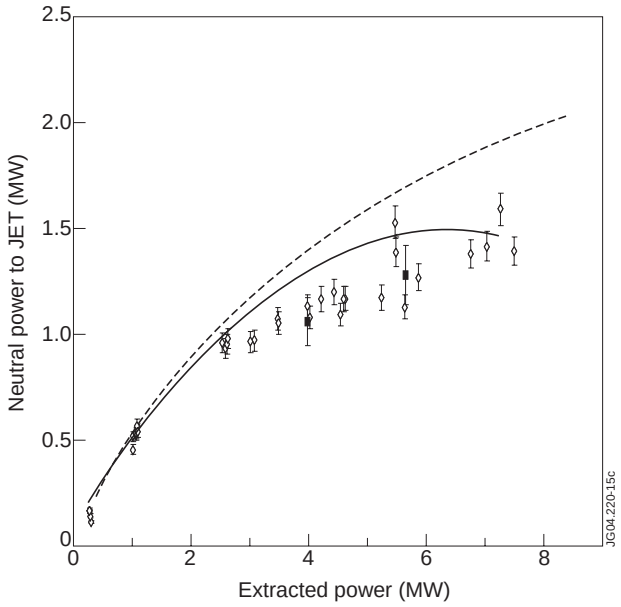

Figure 15: Neutral beam power transmitted to JET as calculated from:------ old target, ◇ measured by calorimetry, ■ measured by plasma response, —— calculated from gas heating model.